

Effect of Long-Range and Local Order of Exfoliated and Proton-Beam-irradiated WSe₂ Nanosheets for Sodium Ion Battery Application

Yu-Gyeong Chun, Won-Jae Lee, Minseop Lee, and Seung-Min Paek*

Department of Chemistry, Kyungpook National University, Daegu 41566, Republic of Korea.

*E-mail: smpaek@knu.ac.kr

Received February 19, 2018, Accepted March 21, 2018

WSe₂ nanosheets were synthesized by mechanical exfoliation via sonication of bulk WSe₂ in organic solvent. The exfoliated WSe₂ nanosheets were separated into two different particle size ranges, and were then irradiated by a proton beam for modification of their local structure, along with the original bulk sample. According to X-ray diffraction (XRD) and X-ray absorption spectroscopy (XAS) analyses of the samples, the mechanical exfoliation reaction mainly affected the long-range order of the WSe₂ samples, whereas proton beam irradiation influenced the local structure of the two-dimensional WSe₂. To examine the structural dependence of exfoliated and proton-beam irradiated WSe₂ in sodium ion battery (NIB) applications, charge/discharge experiments were carried out, which showed that proton beam irradiation could effectively enhance both the discharge capacity and cycling performance of the WSe₂ samples. This synthetic procedure via proton beam irradiation is expected to be used for the development of new anode materials with increased energy density in NIBs.

Keywords: Layered WSe₂, Sodium ion battery, Proton beam irradiation, X-ray absorption spectroscopy

Introduction

Lithium ion batteries (LIBs), as rechargeable batteries, have attracted much research interest from scientists as well as industry, and are soon becoming a mainstream technology for mobile and automotive applications owing to their promising properties such as high energy density and good durability.^{1,2} Although there is currently a stable supply of lithium, there might be a lithium shortage in the near future because of uneven distribution and insufficient supply.^{3,4} As the demand for sustainable energy storage devices increases, sodium ion batteries (NIBs) could be one of the alternatives for secondary batteries, because sodium is abundant, low in cost, and similar to lithium in terms of its physicochemical properties. Most cathode materials for LIBs, such as layered transition metal oxides, can be used for NIBs, since lithium intercalation chemistry is applicable in a similar way to a cathode in NIBs.⁵ However, graphite, which is commonly used as an anode in LIBs, cannot intercalate sodium ions in electrochemical cells, because a sodium ion is 55% larger than that of lithium.⁶ In this regard, there is urgent need to identify new anode materials for NIBs with high energy density.

Transition metal-containing anodes for NIBs could be one of the reliable alternatives, because they can accommodate very large amounts of sodium ions via a conversion reaction.⁷ In particular, transition metal dichalcogenides (MX₂, where M = Mo, W, Nb and X = S, Se, Te) tend to have a layered structure due to weak van der Waals interactions between adjacent sheets. Therefore, sodium cations

are easily accessible to the intersheet region of transition metal dichalcogenides owing to the large interlayer spacing, even though transition metal dichalcogenides have a similar lamellar structure (space group P6₃/mmc) to graphite. We chose tungsten diselenide (WSe₂) as a representative example for anodes in NIBs, because WSe₂ has quite a large interlayer spacing of 0.65 nm between adjacent selenium ions.⁸ Even though a reaction mechanism for the charge/discharge of anodes in NIBs is quite complex and still under debate, it is known that a transition metal dichalcogenide, such as WSe₂, follows conversion and alloying reactions for sodiation/desodiation.⁹ However, WSe₂ has an inherent limitation of rapid volume expansion and capacity fading in the process of charge/discharge of sodium ions, which are larger than lithium ions.¹⁰ In order to overcome this limitation, we have attempted to examine the effect of morphological changes of WSe₂ in NIBs, because the size of the primary particle could have a significant influence on the charge/discharge process. To date, numerous studies have been devoted to the development of anode materials in NIBs; however, systematic studies to examine the effect of the lateral size of lamellar materials are quite scarce. WSe₂ can be a good candidate for reducing its particle size, because it can be exfoliated into single sheets and separated into different fractions by centrifugation depending on the lateral size, as shown in the schematic illustration (Figure 1). A key strategy in this study was to synthesize macroporous WSe₂ of different lateral sizes and thicknesses without any deterioration of the crystal and electronic structure of 2H-WSe₂. The effect of a structural disorder in the

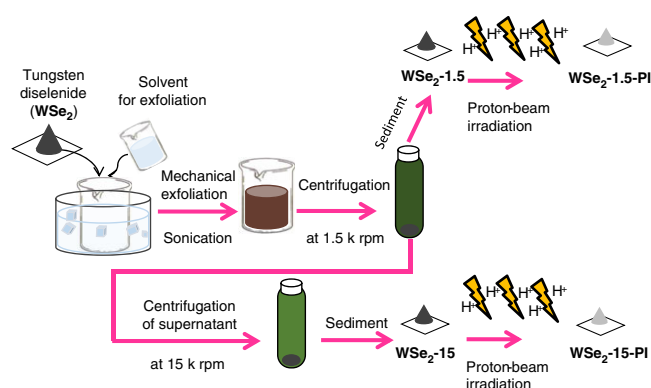


Figure 1. Schematic illustration of the sample synthesis using exfoliation, subsequent self-restacking, and proton-beam irradiation.

short-ranged region was also examined by the introduction of local structural variations using ion beam irradiation. High energy proton beams from a cyclotron and/or linear accelerator could provide enough energy to induce defect sites and/or local disorder in electrode materials for NIBs.¹¹ The discharge capacity and cyclic performance of the samples upon sodium ion storage were compared in order to understand the effects of changes in the particle size and local structural variation.

Experimental

Sample Preparation and Proton Beam Irradiation. The mechanical exfoliation was conducted by sonication of the bulk WSe_2 (Aldrich, St. Louis, Missouri, USA) in an appropriate solvent as previously described.¹² *N*-cyclohexyl-2-pyrrolidone (CHP), suitable for dispersing WSe_2 , was used as solvent for mechanical exfoliation. WSe_2 powder was put into CHP at the concentration of 40 mg/mL, followed by ultrasonic treatment using a horn probe sonication tip for 1 h at the power of 750 W (SONICS Vibra-Cell VCX 750, Newtown, CT, USA). In order to separately collect the exfoliated WSe_2 nanosheets according to the particle size, the colloidal dispersion of WSe_2 was centrifuged at the rpm of 1.5 k for 30 min. After the sediment was washed with acetone, the first sample (WSe_2 -1.5) was obtained, which had smaller lateral size than the bulk WSe_2 . By further centrifuging the supernatant at the rpm of 15 k for 30 min, the second sample (WSe_2 -15) with the smallest lateral size was collected.

Proton beam irradiation was used to induce local structural disorder of samples. Each sample was irradiated with proton beam by using the MC-50 cyclotron at the Korea Institute of Radiological and Medical Sciences (KIRAMS) and/or proton beam accelerator (TR102) in Korea Multi-purpose Accelerator Complex (KOMAC). Three kinds of samples such as bulk WSe_2 , WSe_2 -1.5, and WSe_2 -15, were dispersed in isopropyl alcohol at the concentration of 15 mg/mL, respectively. And then, each dispersion was

exposed to proton beam bombardment at room temperature for 1 h, in which the proton beam energy was 7 MeV. Hereafter, three kinds of samples (bulk WSe_2 , WSe_2 -1.5, and WSe_2 -15) after proton-beam irradiation (PI) were abbreviated as WSe_2 -PI, WSe_2 -1.5-PI, and WSe_2 -15-PI, respectively. Total dose for proton beam irradiation was adjusted to the 3.2×10^{11} particle/cm². Proton beam irradiation using TR102 was conducted with pelletized samples in ambient atmosphere.

Sample Characterization. The crystal structures of products were examined by X-ray diffractometer (XRD, Bruker D2 phaser, Billerica, MA, USA) using Cu $K\alpha$ radiation ($\lambda = 1.5418 \text{ \AA}$). The X-ray absorption spectroscopy (XAS) including the X-ray absorption near edge structure (XANES) and the extended X-ray absorption fine structure (EXAFS) was conducted by using the 8C beamline of Pohang Accelerator Lab (PAL) in Pohang, Korea. The XAS analysis at W L3-edge and Se K-edge was carried out by the standard procedure as described previously.^{13–15} The morphological evolution of products was probed by using scanning electron microscope (SEM, Hitachi SU-8220, Tokyo, Japan) and transmission electron microscope (TEM, Hitachi HT-7700, Tokyo, Japan).

Charge/Discharge Experiments. To evaluate sodium storage property of samples, electrochemical charge/discharge experiments were carried out with battery test equipment (Maccor K4300, Tulsa, Oklahoma, USA). About 70% active material, 25% conductive carbon (Super P), and 5% polyacrylamide were mixed in *N*-methyl-2-pyrrolidone (NMP). The obtained slurry was casted onto copper foil by doctor blade, followed by drying under vacuum at 100°C overnight, and introduced into an Ar-filled glovebox without any exposure to air. Standard CR2032-type coin cell was constructed with the active electrode and sodium foil counter electrode, in which 1 M NaClO_4 in propylene carbonate was used as an electrolyte. A constant current with a current density of 50 mAh/g was applied for charge/discharge experiment, in which a voltage window was between 0.01 and 2.0 V.

Results and Discussion

Figure 2(a) shows XRD patterns of the exfoliated and self-reassembled WSe_2 derivatives after mechanical exfoliation in CHP solvent, along with the bulk WSe_2 for comparison. WSe_2 with lamellar structure was exfoliated in CHP, following which exfoliated WSe_2 with different particle sizes was collected by controlling the speed of centrifugation. The XRD pattern of bulk WSe_2 can be indexed to a space group of $P6_3/mmc$ with a hexagonal unit cell.¹⁶ The cell parameters of $a = 3.282 \text{ \AA}$ and $c = 12.961 \text{ \AA}$ after least-squares refinement are in good agreement with those in a previous report.¹⁷ The basal spacing of bulk WSe_2 was 6.51 Å, calculated from the (002) peak appearing at $2\theta = 13.6^\circ$. After exfoliation and subsequent self-restacking with centrifugation at 1.5 k rpm, the intensity of the (002) peak of WSe_2 -1.5 was slightly decreased, indicating a

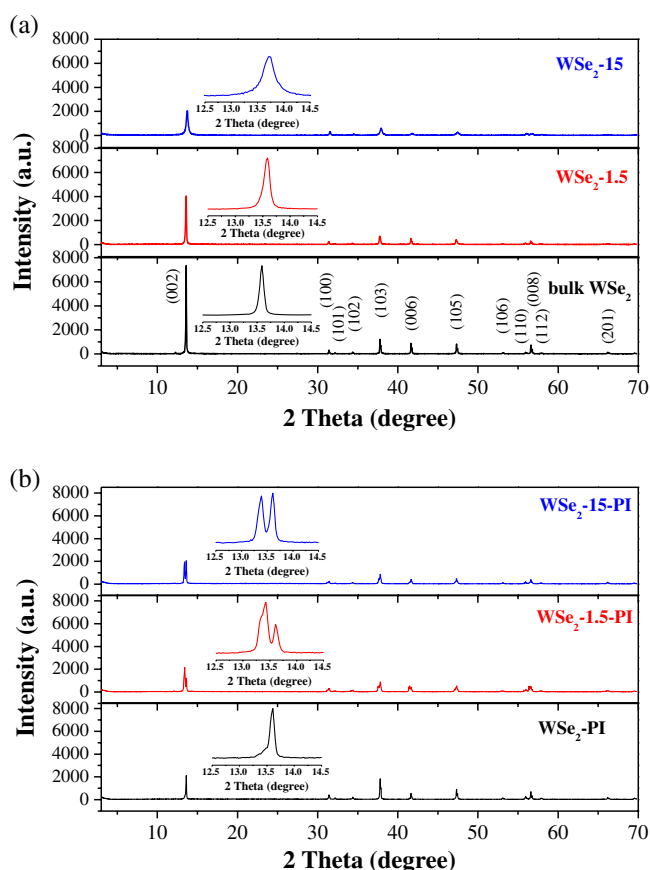


Figure 2. XRD patterns of (a) the bulk WSe₂ and self-restacked WSe₂ derivatives and (b) samples irradiated by proton beam (inset: Enlarged XRD patterns in the range of 12.5–14.5°).

smaller lateral size of WSe₂-1.5 compared to that of bulk WSe₂. The (002) peak intensity of WSe₂-15 is approximately 37% of that of bulk WSe₂, whereas the full width at half maximum (FWHM) of WSe₂-15 is much larger than that of bulk WSe₂. Such an XRD result highlights the smaller particle size of WSe₂-15 due to disorder in the long-range region caused by exfoliation. From this result, it is expected that the thickness of samples also decreases as the centrifugation speed increases. The average particle sizes of the samples were estimated by the Debye–Scherrer equation.¹⁸ The particle sizes of bulk WSe₂, WSe₂-1.5, and WSe₂-15, were determined to be approximately 190, 110, and 70 nm, respectively. Although the Debye–Scherrer equation is generally used for evaluating the particle size of globular particles, it is quite certain that the separation of exfoliated WSe₂ was well-performed with respect to their particle sizes. When we compared the intensity ratios (I_R) of the (100) peak to those of the (002) peak, the I_R values were 0.17, 0.16, and 0.04 for bulk WSe₂, WSe₂-1.5, and WSe₂-15, respectively. This result confirms that *in*-plane ordering of the samples also decreases as the particle size of the samples decreases. Moreover, when the XRD peaks at above 30° are compared, we can observe decreased XRD intensity and broadened FWHM as the particle size

decreases. These phenomena are due to structural disorder in the *in*-plane direction, caused by weakened van der Waals interactions between the adjacent layers and disturbance of the atomic arrangement in WSe₂ layers. Such a result is due to destructive interference from diffracted X-ray waves, caused by long-range disorder of WSe₂ after exfoliation and a restacking reaction.

Figure 2(b) shows XRD patterns for the samples after ion beam irradiation. For all the proton-beam-irradiated samples, the overall intensities of XRD peaks decrease when compared to those before proton beam irradiation. It is worthwhile to note that the (002) peaks in WSe₂-1.5-PI and WSe₂-15-PI appearing at 13.6° are divided into two peaks appearing at 13.4° and 13.6°, suggesting that WSe₂-1.5-PI and WSe₂-15-PI contain different repeating distances after proton beam bombardment. The (002) peak in WSe₂-PI shows a much broader shape on the lower angle side. These changes in the intensities and shapes of the (002) XRD peaks after proton beam irradiation are ascribed to structural disorder of the lattices along the crystallographic *c*-axis, because an energetic proton beam could provide the high energy necessary for atomic displacement.

Direct evidence for structural changes arising from the exfoliation and proton beam treatment was obtained from SEM and TEM analysis (Figure 3). The left-side and right-side figures are before and after proton beam irradiation, respectively. Bulk WSe₂ was composed of the largest particles, having widths ranging from 10 to 50 μm, whereas the lateral size of WSe₂-1.5 was below 20 μm. The insets in Figure 3(a), (c), and (e) show the edge-side of each sample, in which stacking between adjacent layers can be observed. The thicknesses of the samples gradually reduce as the lateral particle size decreases. The WSe₂-15 sample consisted of very small flakes, in which the widths of the primary particles were below 1 μm. Moreover, in the WSe₂-15 sample, very small and thin plates were stacked with irregular patterns, showing that these plates are composed of self-restacked layers after a full degree of exfoliation. As shown in Figure 3(g), TEM images for the self-restacked WSe₂-15 indicated very thin nanosheets with pale contrast, showing the fully exfoliated nature of WSe₂-15. The thin nature of WSe₂-15 is also observed after proton beam irradiation (Figure 3(h)), in which the basal spacing between adjacent layers can be observed as seen in the inset. The overall morphology for all the proton-beam-irradiated samples such as WSe₂-PI, WSe₂-1.5-PI, and WSe₂-15-PI (Figure 3(b), (d), (f), and (h)) is quite similar to those before ion beam treatment. However, the particle sizes of proton-beam irradiated samples were slightly smaller than those of the samples before proton-beam irradiation, implying that proton beam bombardment affects both the local structure and macromolecular characteristics.

To investigate local structural and electronic features of samples upon the exfoliation and the proton beam irradiation, we performed X-ray absorption spectroscopy (XAS) analysis such as the extended X-ray absorption fine

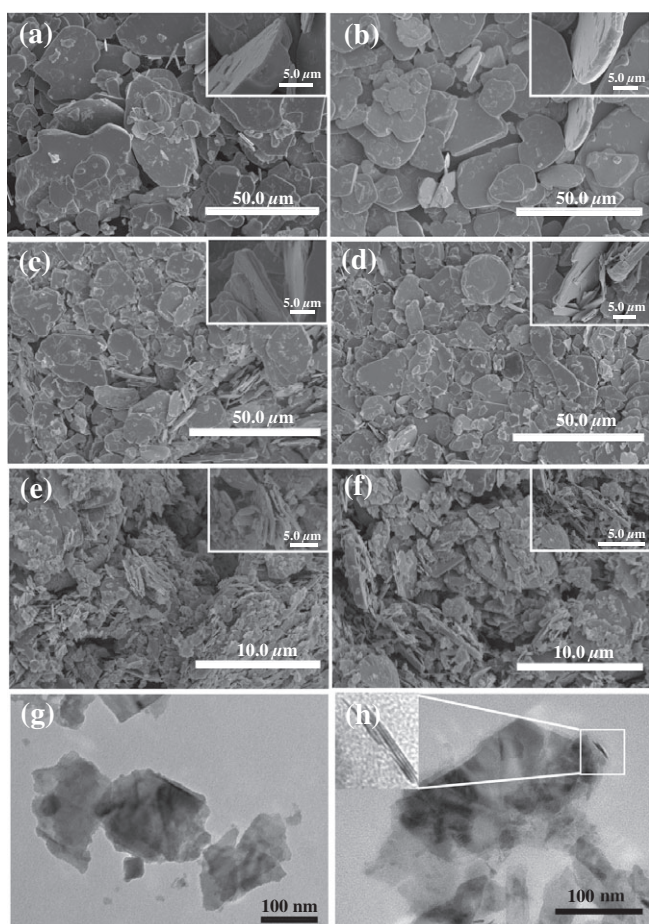


Figure 3. SEM and TEM images of samples before and after ion beam irradiation: The left side figures ((a), (c) and (e)) represent SEM images for bulk WSe_2 , WSe_2 -1.5, and WSe_2 -15 samples, respectively, while the right side figures ((b), (d), and (f)) are SEM images of WSe_2 -PI, WSe_2 -1.5-PI, WSe_2 -15-PI samples after ion beam irradiation. (g) and (h) represent TEM images for WSe_2 -15 and WSe_2 -15-PI after ion beam irradiation.

structure (EXAFS) and X-ray absorption near edge structure (XANES) as shown in Figure 4. In XANES spectra at W L_3 -edge (Figure 4(a)), white lines are mainly ascribed to the electronic transitions from $2p_{3/2}$ to vacant $5d$ orbitals.¹⁹ The threshold energy of main edges of samples at W L_3 -edge was shifted to the higher energy position after proton beam irradiation, revealing that tungsten atoms in WSe_2 samples were slightly oxidized by proton beam. This result implies that the proton beam treatment induced local structural stresses for WSe_2 samples, which is in good agreement of XRD results showing the increased basal spacing after proton beam irradiation. Se K-edge XANES spectra (Figure 4(b)) also showed shifted main edges to the higher energy. It was found that the ion beam comprising H^+ cations caused oxidation of not only tungsten but also selenium atoms in the WSe_2 frameworks. The extent of oxidation could be estimated by the edge position, which displays that the oxidative tendency of in WSe_2 -1.5 and

WSe_2 -15 was much larger than that of the bulk WSe_2 . WSe_2 -1.5 and WSe_2 -15 consisting of smaller particles have much larger amount of exposed atoms on the surface, leading to easier oxidation of atoms than those in bulk state. Meanwhile, overall shapes of XANES spectra after proton beam irradiation is quite analogous to those before proton beam treatment, suggesting that electronic structures of samples were not deteriorated by proton beam.

Figure 4(c) and (d) display radial distribution functions (RDFs) of k^3 -weighted EXAFS signals (non-phase-shift-corrected), which were obtained from the Fourier

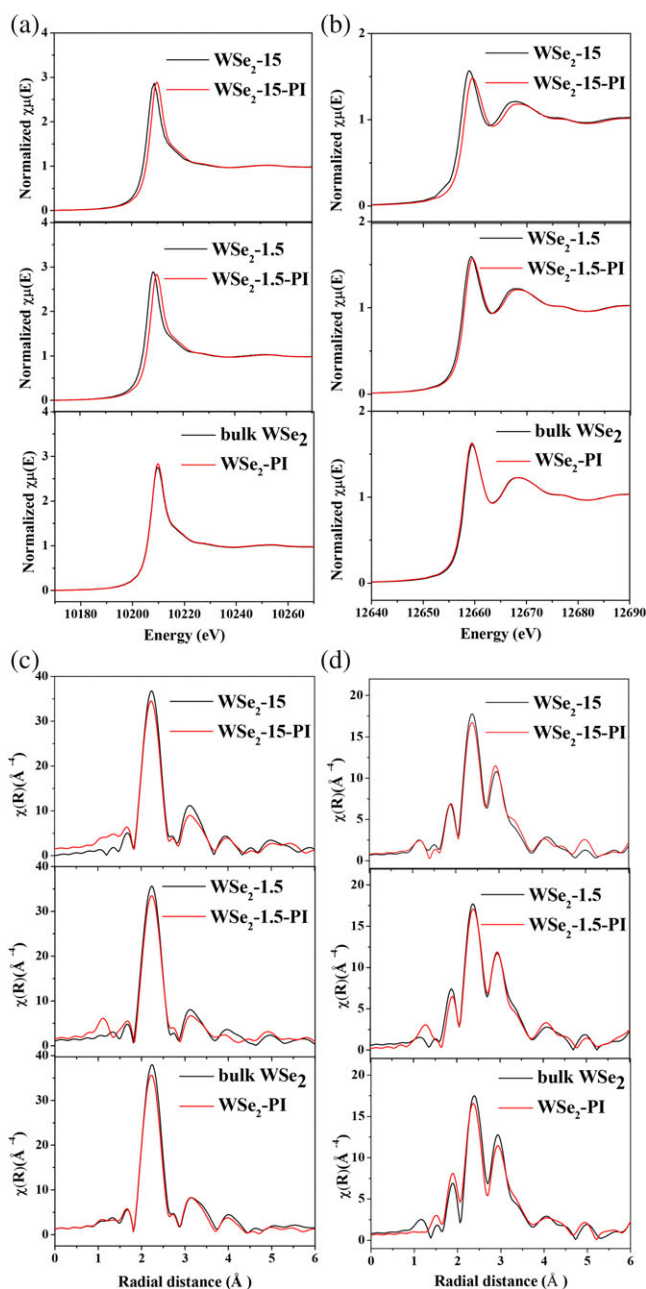


Figure 4. XANES spectra of samples at (a) W L_3 -edge and (b) Se K-edge. Radial distribution function (RDF) of Fourier-transformed (FT) EXAFS signal for samples at (c) W L_3 -edge and (d) Se K-edge.

Transformation. In the RDFs at W L₃-edge (Figure 4(c)), the first FT peak appearing around 2.3 Å is assigned to the first neighboring Se atoms covalently bonded to W atoms, while the second peak near 3.1 Å, relatively smaller peak than the first one, is due to the W atoms in the second neighboring shells from the absorbing W atoms.²⁰ Since anisotropic interaction between Se atoms is rather stronger than that between the other elements in WSe₂,^{21,22} the FT amplitude of the second shell had much smaller than that of the first shell. In addition, Figure 4(d) shows the local fine structural features at Se K-edge. Here, two kinds of strong peaks are shown, in which the first FT peak at 2.4 Å is covalently bonded Se atoms and the second FT peak at 2.9 Å is assigned to the nearest W atoms. According to RDF spectra, overall local structures of samples were preserved even after the proton beam treatment, however, the intensities of the first peak owing to the chemical bonds between W and Se were slightly decreased after proton beam irradiation. This reduced amplitude of the first shell is attributed to the disturbance and/or variation in bond length of (W–Se), as a result of local disorder introduced by proton beam. From the above XAS analysis, it is certain that ion beam could control the local structures of WSe₂ samples, leading to the displacement and/or structural disorder of W and Se atoms induced by energetic proton beam.

To evaluate the electrochemical performance of the prepared samples before and after proton beam irradiation, half cells of the samples were assembled for NIB application, and their galvanostatic charge/discharge experiments were performed at a current density of 30 mA/g and in the cutoff voltage range of 0.01–2.0 V (Figure 5). The sodiation and desodiation mechanism in NIBs is still under debate; however, the first discharge curve is ascribed to the sodium intercalation reaction and/or conversion reaction as shown in Figure 5 (a–c). The reversible discharge capacity of the bulk WSe₂ was 270 mAh/g at the second discharge as seen in Figure 5(d). This discharge capacity of the bulk WSe₂ slowly faded to 120 mAh/g after the 30th cycle, which was only approximately 44% retention of the reversible discharge capacity. Such a large capacity fading upon successive charge/discharge is due to the formation of a solid-electrolyte interphase (SEI), incomplete conversion reaction, and electrolyte reduction during cycling.^{23–25} After proton beam irradiation, WSe₂-PI had a reversible discharge capacity of 270 mAh/g, similar to that of bulk WSe₂ itself. However, the discharge capacity of WSe₂-PI after 30 cycles was 170 mAh/g, or 63% of the reversible capacity. Such an enhancement in cyclability implies that proton beam irradiation could be used as an effective method to relieve capacity fading. As seen in the SEM and XAS results, a high energy proton beam can modify both the morphology and local structure of WSe₂ and its derivatives. Since proton-beam-irradiated samples have much higher flexibility than unirradiated samples, local disorder of samples after proton beam bombardment facilitates facile and reversible sodiation and desodiation, leading to an

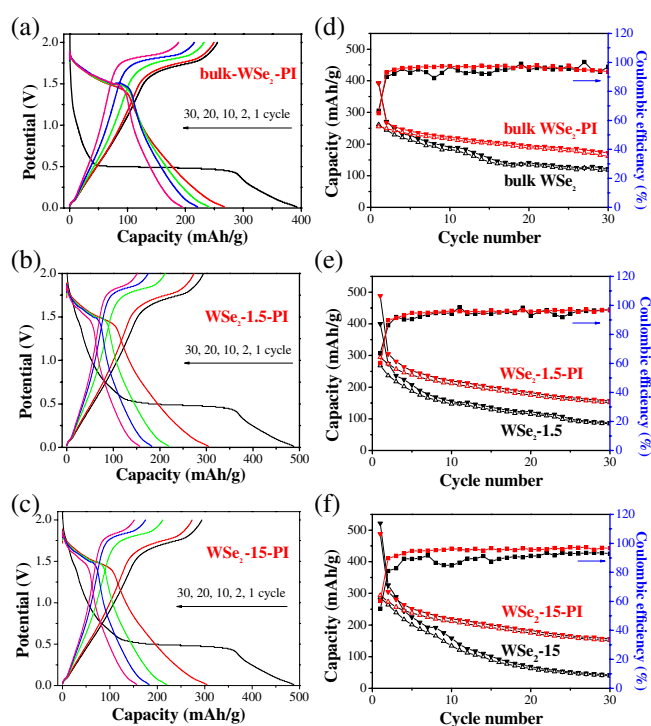


Figure 5. Charge/discharge curves of (a) bulk WSe₂-PI, (b) WSe₂-1.5-PI, and (c) WSe₂-15-PI after proton beam irradiation. The cycling performance of (d) bulk WSe₂, (e) WSe₂-1.5, and (f) WSe₂-15 before and after proton beam irradiation (filled triangle: discharge capacity, empty triangle: charge capacity, square: Coulombic efficiency).

enhanced cyclability. Similar increased discharge capacity was also found in WSe₂-1.5 after proton beam irradiation, as shown in Figure 5(e). WSe₂-15, with the smallest particle size among the samples, exhibited the largest first discharge capacity because of additional sodiation via SEI formation. However, the charge/discharge experiment for WSe₂-15 revealed that it had a very small discharge capacity of 40 mAh/g at the 30th cycle, due to a low Coulombic efficiency, as seen in Figure 5(f). After the proton beam treatment, the discharge capacity of WSe₂-15-PI was 160 mAh/g, which is four times larger than that before proton beam irradiation. It is highly plausible that local structural defects developed via proton beam treatment can be used as buffer spaces during volume changes upon successive sodiation/desodiation, leading to increased cyclability. Among the three WSe₂ samples, WSe₂-15 showed the highest increase in discharge capacity after proton beam treatment. Such a result is possibly due to the smallest particle size, largest surface area, and the most disordered structures of WSe₂-15. The large flexibility of WSe₂-15 could facilitate the efficient development of buffer spaces via ion beam treatment, leading to the enhanced electrochemical properties. In case of the bulk WSe₂-PI irradiated by proton beam accelerator (not shown), discharge capacity was nearly similar to that before irradiation, even though the same total dose was used for the proton beam irradiation. This suggests that the pulsed beam from accelerator in

ambient atmosphere affected little on the local structure. In case of proton beam irradiation on samples in ambient atmosphere, radiolysis of solvents could not happen, resulting that no discernible change in the oxidation states of each ions in WSe₂.

Conclusion

It was demonstrated that proton beam irradiation can be used for the development of new anode materials with increased cyclability for NIB applications. According to XRD and XAS results, the long-range order of crystals can be controlled by mechanical exfoliation of WSe₂ whereas the local structure of WSe₂ is modifiable by proton beam irradiation. Electrochemical charge/discharge experiments of the samples clearly revealed that the discharge capacity and cyclability of the samples were enhanced after proton beam treatment, emphasizing that the present synthetic route using proton beam treatment could be extended to the fabrication of new nanostructured NIB electrodes with enhanced electrochemical properties.

Acknowledgments. We gratefully acknowledge financial support from the National Research Foundation of Korea (NRF: 2016M2B2A4912195, 2017M2B2A4049463, and 2015R1D1A3A01016279). This work was also partly supported by Dongil Culture and Scholarship Foundation of Korea.

References

1. N.-S. Choi, Z. Chen, S. A. Freunberger, X. Ji, Y.-K. Sun, K. Amine, G. Yushin, L. F. Nazar, J. Cho, P. G. Bruce, *Angew. Chem. Int. Ed.* **2012**, *51*, 9994.
2. H. Li, Z. Wang, L. Chen, X. Huang, *Adv. Mater.* **2009**, *21*, 4593.
3. X. Zeng, J. Li, N. Singh, *Crit. Rev. Environ. Sci. Technol.* **2014**, *44*, 1129.
4. Y. Wen, K. He, Y. Zhu, F. Han, Y. Xu, I. Matsuda, Y. Ishii, J. Cumings, C. Wang, *Nat. Commun.* **2014**, *5*, 4033.
5. I. Hasa, D. Buchholz, S. Passerini, J. Hassoun, *ACS Appl. Mater. Interfaces* **2015**, *7*, 5206.
6. L. Xiao, Y. Cao, J. Xiao, W. Wang, L. Kovarik, Z. Nie, J. Liu, *Chem. Commun.* **2012**, *48*, 3321.
7. F. Klein, B. Jache, A. Bhide, P. Adelhelm, *Phys. Chem. Chem. Phys.* **2013**, *15*, 15876.
8. M. Nath, C. N. R. Rao, *Chem. Commun.* **2001**, *21*, 2236.
9. D. Chao, C. Zhu, P. Yang, X. Xia, J. Liu, J. Wang, X. Fan, S. V. Saviolov, J. Lin, H. J. Fan, Z. X. Shen, *Nat. Commun.* **2016**, *7*, 12122.
10. K. Share, J. Lewis, L. Oakes, R. E. Carter, A. P. Cohn, C. L. Pint, *RSC Adv.* **2015**, *5*, 101262.
11. W. Li, X. Wang, X. Zhang, S. Zhao, H. Duan, J. Xue, *Sci. Rep.* **2015**, *5*, 9935.
12. V. Nicolosi, M. Chhowalla, M. G. Kanatzidis, M. S. Strano, J. N. Coleman, *Science* **2013**, *340*, 1226419.
13. M.-H. Choi, Y.-J. Min, G.-H. Gwak, S.-M. Paek, J.-M. Oh, *J. Alloys Compd.* **2014**, *610*, 231.
14. W.-J. Lee, Y.-G. Chun, S.-J. Jang, S.-M. Paek, J.-M. Oh, *J. Alloys Compd.* **2017**, *711*, 611.
15. Y.-J. Min, W.-J. Lee, G.-H. Gwak, S.-M. Paek, J.-M. Oh, *Bull. Korean Chem. Soc.* **2015**, *36*, 2627.
16. X. Wang, X. Chen, Y. Zhou, C. Park, C. An, Y. Zhou, R. Zhang, C. Gu, W. Yang, Z. Yang, *Sci. Rep.* **2017**, *7*, 46694.
17. W. J. Schutte, J. L. De Boer, F. Jellinek, *J. Solid State Chem.* **1987**, *70*, 207.
18. B. D. Cullity, *Elements of X-Ray Diffraction*, 2nd ed., Addison-Wesley, Reading, MA, **1977**.
19. S. Yamazoe, Y. Hitomi, T. Shishido, T. Tanaka, *J. Phys. Chem. C* **2008**, *112*, 6869.
20. E. Prouzet, J. Heising, M. G. Kanatzidis, *Chem. Mater.* **2003**, *15*, 412.
21. S. M. Heald, E. A. Stern, *Phys. Rev. B* **1977**, *16*, 5549.
22. P. Le Fèvre, H. Magnan, D. Chandesris, *Phys. Rev. B* **2830**, 1996, 54.
23. F. Chen, J. Wang, B. Li, C. Yao, H. Bao, Y. Shi, *Mater. Lett.* **2014**, *136*, 191.
24. K. Chen, W. Zhang, L. Xue, W. Chen, X. Xiang, M. Wan, Y. Huang, *ACS Appl. Mater. Interfaces* **2017**, *9*, 1536.
25. C. C. Nguyen, T. Yoon, D. M. Seo, P. Guduru, B. L. Lucht, *ACS Appl. Mater. Interfaces* **2016**, *8*, 12211.